energies

MDPI

Article

Optimization of Supercapacitor Assisted Surge Absorber (SCASA) Technique: A New Approach to Improve Surge Endurance Using Air-Gapped Ferrite Cores

Sadeeshvara Udayanga Silva Thotabaddadurage *, Nihal Kularatna and D. Alistair Steyn-Ross

School of Engineering, University of Waikato, Hamilton 3240, New Zealand; nihalkul@waikato.ac.nz (N.K.); asr@waikato.ac.nz (D.A.S.-R.)

* Correspondence: sus1@students.waikato.ac.nz or sadeeshvara.udayanga@gmail.com

Abstract: SCASA is a patented technique commercialized as a surge protector device (SPD) that adheres to UL-1449 test standards. Apart from the novel use of supercapacitors, SCASA design incorporates a coupled-inductor wound to a specially selected magnetic material of powdered-iron. In this study, we investigate the limitations of the present design under transient operation and elucidate ways to eliminate them with the use of air-gapped ferrite cores. In modelling the operation under 50 Hz AC and transient conditions, a permeance-based approach is used; in addition, non-ideal characteristics of the transformer core are emphasized and discussed with empirical validations. The experimental work was facilitated using a lightning surge simulator coupled with the 230 V AC utility mains; combinational surge-waveforms (6 kV/3 kA) defined by IEEE C62.41 standards were continuously injected into SPD prototypes during destructive testing. Such procedures substantiate the overall surge-endurance capabilities of the different core types under testing. With regard to optimizations, we validated a 95% depletion of a negative-surge effect that would otherwise pass to the load-end, and another 13–16% reduction of the clamping voltage verified the effectiveness of the methods undertaken. In conclusion, SCASA prototypes that utilized air-gapped cores revealed a greater surge endurance with improved load-end characteristics.

Keywords: supercapacitors; surge protection; magnetic permeance; air-gapped transformer; effective permeability; SCASA

Citation: Silva Thotabaddadurage, S.U.; Kularatna, N.; Steyn-Ross, D.A. Optimization of Supercapacitor Assisted Surge Absorber (SCASA) Technique: A New Approach to Improve Surge Endurance Using Air-Gapped Ferrite Cores. *Energies* **2021**, *14*, 4337. https://doi.org/10.3390/en14144337

Academic Editor: Woojin Choi

Received: 16 May 2021
Accepted: 9 July 2021
Published: 19 July 2021

1. Introduction

Over the last few decades, with the rapid developments in electronics industry, the need for processing and managing electricity has emerged as an essential requirement to obtain disturbance-free power. Based on the developments of international technology roadmap for semiconductors (ITRS) and its predictions, the protection of modern-day electronic systems from high voltage transients has become mandatory [1]. Today, more than 75% of the power generated across the world is processed by power electronics [2]. In a single- or three-phase utility main supply, it is expected that AC power delivers at a nominal RMS voltage with a minimum percentage tolerance of ±5–10% [3].

However, due to voltage disturbances, such as RMS fluctuations, transients, noise, and harmonics, utility power is downgraded. Out of various power quality issues, transient phenomena are considered to have the greatest voltage stress in an electronic system if not properly mitigated [4]. These are commonly caused by switching operations, lightning strikes, and due to partial discharges of faulty power equipment.

Transients and surges are micro- to millisecond order events superimposed on the AC-input waveform and are highly unpredictable in nature. Though 100% elimination is impossible, surge protector devices are engineered to minimize the transmission of transient surge energy [5]. A circuit component is usually damaged due to an over-current or over-voltage; both these two extreme conditions result in transferring greater amounts

of surge energy damaging the particular component. Under normal conditions, electronic devices show the optimum performance when powered from a 230 V/50 Hz utility main; however, degradation begins to occur as the transient voltage spikes superimposed on the AC main pass into the internal circuits via power supply units.

Therefore, an effective SPD must absorb and dissipate the transient related energy within the unit, while continually facilitating the mains electricity flow at the line frequency to the load under protection. Figure 1 illustrates different levels of degradation due to transient surges superimposed on the AC-input. Any spike amplitude above 900 V is highly detrimental [6], whereas 600–900 V is the range where internal degradations start to occur. However, transients below 600 V are usually considered to be safe [6].

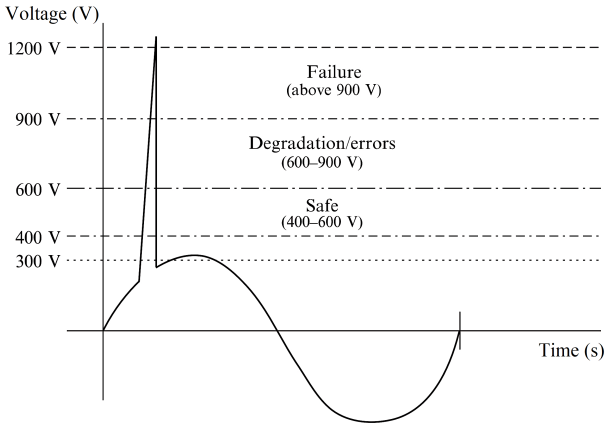

Figure 1. A transient superimposed on AC-input with degradation levels.

In designing circuits for surge absorption, a designer must take into account two main factors: (1) the surge absorber circuit should not disturb the normal AC operation of the connected device, and (2) components used to attenuate the surge must be able to withstand and absorb the surge. All SPD circuits function according to the voltage division principle [7]. Figure 2 depicts the general conceptual design approach to surge absorption by adopting a simple pair of impedances. As per Figure 2a, the load Z_L to be protected comes in series with a small impedance Z_{series}, which represents the Thevenin's impedance of the closed loop, formed by stray line inductance and ohmic resistance, etc.

When a surge occurs, the voltage dividing effect of the Z_L and Z_{series} is such that a larger share of surge appears at the load in a destructive form. Figure 2b shows the case of an impedance Z_{block}, which can show a larger value for the high-frequency components associated with a transient. For example, if an inductance is inserted as Z_{block}, at higher frequencies, the inductive-impedance will dominate. This can help to reduce the impact of transients on the Z_L due to voltage divider action.

Another way to reduce the impact of transience is to insert a shunt-type impedance Z_{shunt} as in Figure 2c, which behaves complimentary to the Z_{block}, where, at high frequency or high amplitude of the incoming surge, the impedance value of the Z_{shunt} decreases. This results in diverting the surge away from the load.

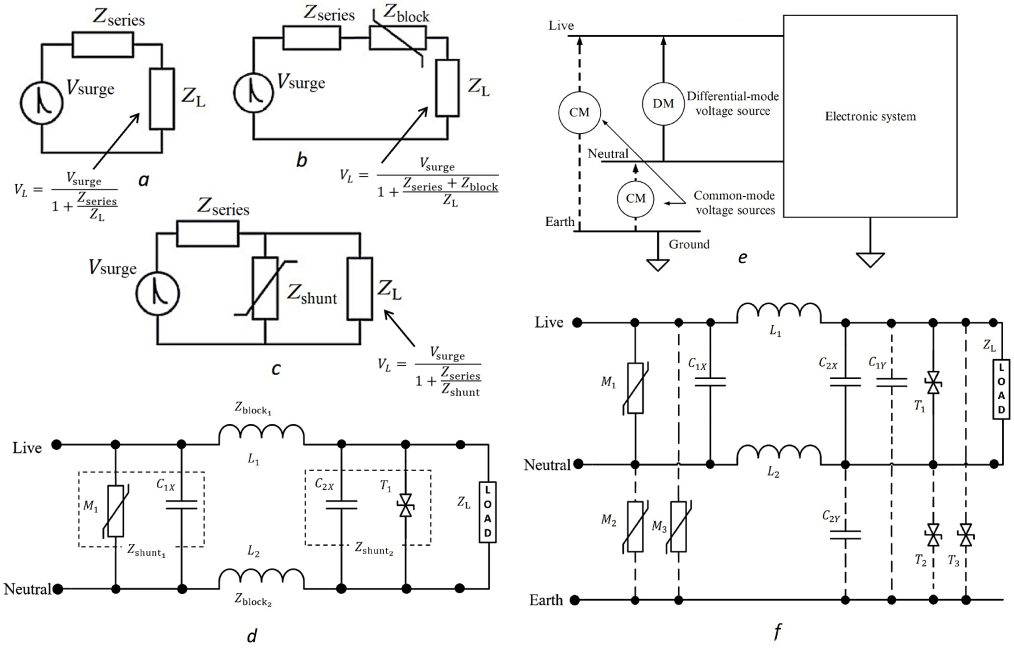

Figure 2. Basic functional types of surge suppressors and their implementation: (**a**) Without any protection element; (**b**) With series blocking element; (**c**) With diversion of the surge using shunt devices; (**d**) A differential-mode surge protector with a series and shunt devices; (**e**) Different modes of signal inputs: differential-mode and common-mode; and (**f**) A typical dual-mode surge protector designed for a three-wire power system.

A traditional surge protector that operates only for differential mode signals (i.e., transient signals appearing between live to neutral wire) is shown in Figure 2d based on series inductors (L_1, L_2), and two shunt elements, Z_{shunt_1} and Z_{shunt_2} [8]. In the case of Z_{shunt_1}, it is a combination of a capacitor C_{1X} (where the impedance $1/wC$ reduces at high frequencies) and a metal oxide varistor (MOV) M_1. The MOV M_1 reduces its resistance at higher voltages in a non-linear fashion. Similarly, Z_{shunt_2} acts as a secondary shunt element, where C_{2X} acts similar to C_{1X}, with the bidirectional break-over diode (BBD) T_1, which acts non-linearly at a higher speed compared to MOV. More details about how non-linear devices (NLDs), such as MOVs and BBDs, are used in SPDs are available in [9,10].

As transients can appear in both differential and common modes (as depicted in Figure 2e), an advanced SPD must carry much larger combinations of these series and shunt protective elements. Figure 2f is a typical surge protector designed for a three-wire (live, neutral, and earth) power system incorporating both modes of protection, where the circuit parts shown in dotted lines are for common mode transient absorption. More information on this is found in [11,12].

While traditional SPDs are designed using NLDs and inductor capacitor filter combinations as shown in Figure 2f, the use of supercapacitors (SCs) in SPDs is a relatively new concept developed and tested by the power electronics research group at the University of Waikato. According to the investigations summarised in [13], a SC-based low-component count surge protector was developed as SCASA [14–16]. This is a patented technique, which led to a commercial product SMART TViQ, developed and manufactured by Thor technologies, Australia in 2016 [17].

Our research has two prime goals: to optimize the overall performance of the SCASA technique by reducing its load-side voltage and to improve its ultimate surge endurance. This paper is structured into eight sections to achieve these goals. Section 2 focuses on the SC surge absorption capability, while Section 3 describes the operation and limitations of the present SCASA design. In Section 4, we develop models to predict the properties of air-gapped toroidal cores. Using a permeance model, we examine the equivalent circuit of SCASA transformer core in Section 5.

Theoretical predictions are made to analyse different operational modes. Section 6 covers the practical measurements of various non-ideal characteristics of the transformer core, and provides comparisons for the core types tested. Overall circuit improvements validated by LSS-6230 surge tests are discussed under Section 7. An assessment of surge-endurance under repeated surges further justifies the research methods undertaken. Finally, our concluding remarks are given in Section 8.

2. Supercapacitors for Surge Absorption

Electrical double-layer capacitors (EDLCs) were the first SCs to emerge. With a million-times larger capacitance compared to electrolytic capacitors of the same volume, they emerged as prominent energy storage devices. EDLCs have a very low equivalent series resistance (ESR) and a low DC voltage (about 2–4 V) rating [18]. Surprisingly, EDLCs are capable of surviving transient surge pulses of several thousand volts [13,19]. In this Section, we present a surge-based model to justify how EDLCs can withstand transient energies.

The simple model, we discuss here how surge energy is distributed among the resistive and capacitive components of an *RC* circuit during a rectangular surge pulse of time interval T (10 µs). Figure 3a illustrates the capacitance (C) of the SC, the ESR (R) of the SC, and the path resistance (R_P) of the connecting wires. As indicated in Figure 3b, the SC has an extended charging curve (larger time-constant) compared to an electrolytic capacitor (EC); hence, during a surge pulse, the voltage build up across a SC (v_{sc}) is comparably small.

Significantly, v_{sc} is typically much smaller than the rated voltage of a SC, giving it a better chance of survival under a high-voltage pulse. However, in the case of a standard capacitor, the developed voltage (v_c) can be higher than its rated voltage, leading to the failure of the device. The following equations quantify the energies distributed between capacitive and resistive circuit elements during a transient pulse.

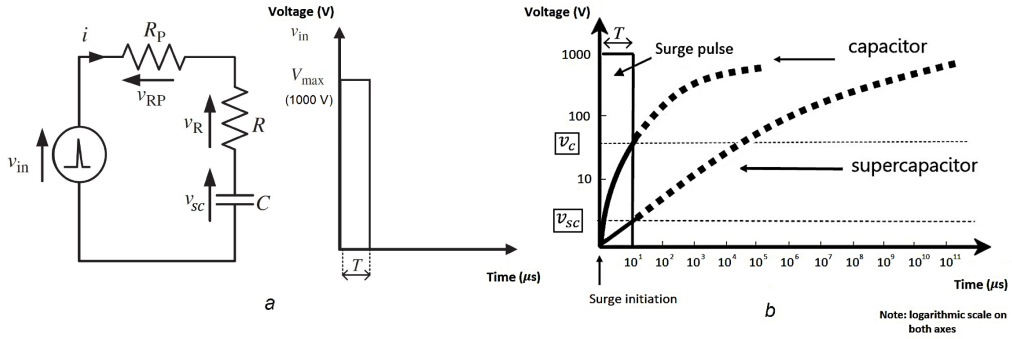

Figure 3. RC circuit subjected to a rectangular high voltage pulse: (**a**) Equivalent circuit of a SC with path resistance and step voltage pulse; (**b**) Supercapacitor vs. capacitor (comparison of voltage build-up).

$$E_{sc} = \frac{1}{2} C {v_{sc}}^2 \tag{1}$$

$$v_{sc} = V_{max}(1 - e^{-t/CR_T}) \tag{2}$$

(1) shows the energy accumulation of the SC as the voltage (v_{sc}) across its terminals varies according to (2). The surge pulse in this example has a maximum voltage (V_{max}) of 1000 V.

Energy dissipated in the ESR (R) of SC due to surge current i ($i = {V_{max}(e^{-t/CR_T})}/{R_T}$) is given by the integral in (3), where R_T refers to the total series resistance ($R + R_P$).

$$E_R = \int_0^T i^2 R \, dt = \frac{CR}{2R_T} V_{max}^2 (1 - e^{-2T/CR_T}) \tag{3}$$

Using (1)–(3), consider the ratio E_R/E_{sc} after time T:

$$\frac{E_R}{E_{sc}} = \frac{R}{R_T}\frac{(1+e^{-T/CR_T})}{(1-e^{-T/CR_T})} \tag{4}$$

When $R = 170$ mΩ, $R_T = 2.17$ Ω, $C = 5$ F and $T = 10$ µs,

$$\frac{E_R}{E_{sc}} \approx 10^5 \tag{5}$$

A key result comes from (4) and (5), which suggests that a greater amount of surge energy is dissipated in ESR while only a minor amount is sunk into the SC. This result further confirms how SCs can withstand transient activities. Similarly, if the path resistance is significant, then a substantial amount of transient energy will be dissipated as heat across the resistive path wires.

Our transient voltage tests confirm that SCs develop fairly insignificant voltages compared to ECs. A comparison of this phenomenon is shown in Figure 4 with two distinct regions for the two types of capacitors. From micro-farad level ECs to farad-level SCs, there is a substantial difference in the accumulated capacitor voltages. Normal capacitors (ECs) develop several thousands of volts when subjected to a 6 kV surge, whereas SCs develop only a few volts—in most cases, several millivolts.

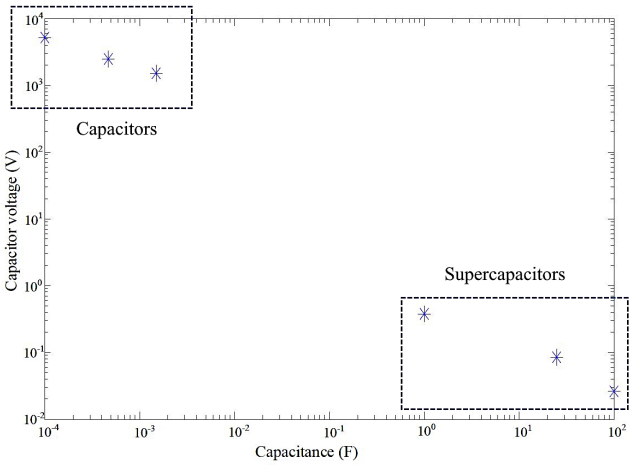

Figure 4. Voltage build up of capacitors and supercapacitors for a 6 kV, 1.2/50 µs surge pulse.

The remarkable surge endurance of SCs is clearly relevant to surge protection applications; however, the main drawback is their low DC voltage rating (≈2.7 V). The low DC rating makes SCs unfit for direct application to 230 V AC utility mains. To address this limitation, the Waikato power electronics team designed a coupled-inductor topology to allow SCs to be incorporated into a practical surge protector. A detailed discussion about the development of this new design is presented next.

3. SCASA Technique

3.1. Implementation of the Coupled-Inductor

Despite the low DC rating of SCs, their large time-constant is an essential property for handling transient events. However, they cannot be used as a direct replacement to typical surge absorbing elements like MOVs or BBDs. However, inductors, when connected in series, can reduce the impact of high frequency components without impeding the passage of the low-frequency (50 Hz) mains component.

In developing SCASA, a coupled-inductor approach was adopted by utilizing a toroidal core with two windings (Figure 5), which partly exhibit transformer properties during surge propagation. The windings are configured in such way that the primary arm

with six turns (N_1) provides a lower impedance path than the secondary with 28 turns (N_2) during the propagation of a surge. The combined action of coupled-inductor windings protects the critical load by storing most of the surge energy magnetically within the toroidal core.

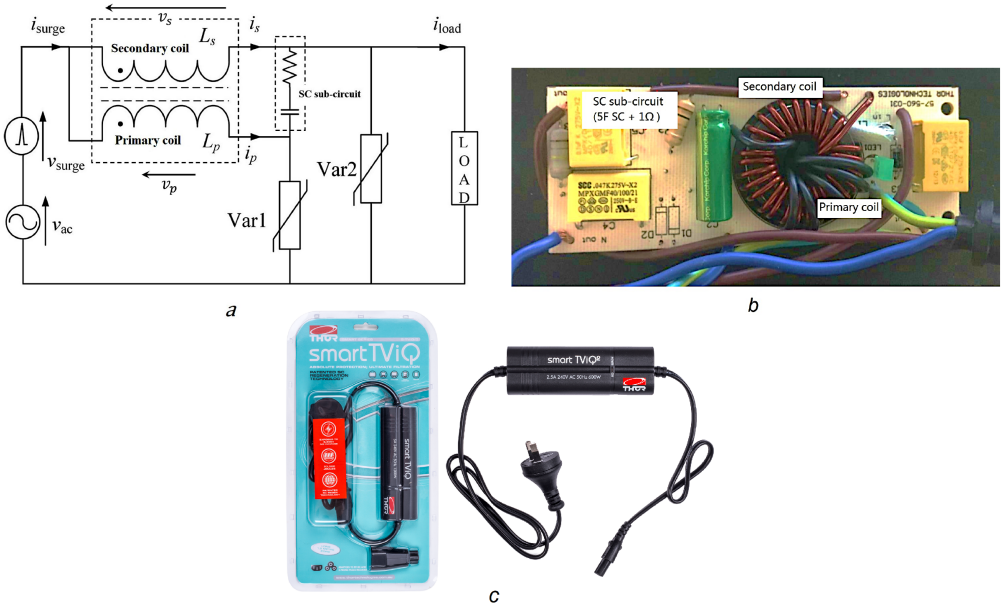

Figure 5. SCASA circuit diagram and real view of the components: (**a**) Circuit diagram of SCASA design; (**b**) SCASA transformer core with coupled-inductor windings and SC sub-circuit and associated components; and (**c**) Commercial implementation of SCASA as a SMART TViQ [17].

The second significant feature is the inclusion of a supercapacitor based sub-circuit. A 1 Ω high power resistor and a 5 F SC connected serially are placed between the ends of two coils to ensure that the voltage across the sub-circuit never exceeds the DC rating of a SC. Therefore, any possibility of damaging the SC is prevented. Moreover, as shown in Figure 5a, the SCASA circuit holds two MOVs (Var1 and Var2) to dissipate the excess surge energy while clamping the voltage transient to a safe level.

Though the circuit has a simple form, the transformer core of SCASA possess several non-ideal characteristics, including magnetizing inductances L_1 & L_2 as well as leakage inductances l_1 & l_2 of both primary and secondary windings (Figure 9). In Section 5, we develop a descriptive model to investigate these characteristics in depth.

In the case of an ideal inductor core, leakage inductances are considered as near zero, and magnetizing inductances are almost infinite; however, since a powdered-iron core is utilized in SCASA, there are significant operational changes that push SCASA into the non-ideal domain. The original powdered-iron core (0077071A7-Magnetics Inc., Pittsburgh, PA, USA) has an initial relative permeability (μ_r) of 60 [20], which is much smaller than the near infinite permeability of ideal magnetic materials. As previously mentioned, the authors aimed at optimizing the overall performance of SCASA technique using ferrite-based toroids.

Materials like laminated ferrite are considered to have ideal magnetic characteristics as they possess extremely high relative permeabilities in the range of 1000–10,000 [21]. The W ferrite material used in this study is a high permeability material with an initial μ_r of 10,000 [22]. In powdered-iron, the permeability is greatly reduced by distributing micro-sized air-gaps inside the material, and a similar effect can be achieved if an external air-gap is introduced to a ferrite-core body [23]. This alters the magnetic reluctance of the core; a detailed discussion about the impact of air-gaps on magnetic materials is presented in Section 4.

In addition to their contrasting permeabilities, powdered-iron and ferrite-iron show significant differences in their hysteresis behaviour (Figure 6). Iron-powder (μ_r = 60) reached magnetic saturation at a relatively higher level (1.0 T, 64,000 A/m) compared to W and H ferrite materials (0.23 T, 25 A/m) at 25 °C [20,21]. This suggests that iron-powder possesses a greater hysteresis area than ferrites. A larger hysteresis loop area corresponds to larger energy losses during magnetization and demagnetization. Therefore, heat dissipation during a hysteresis cycle is more dominant in iron-powder than in ferrite materials.

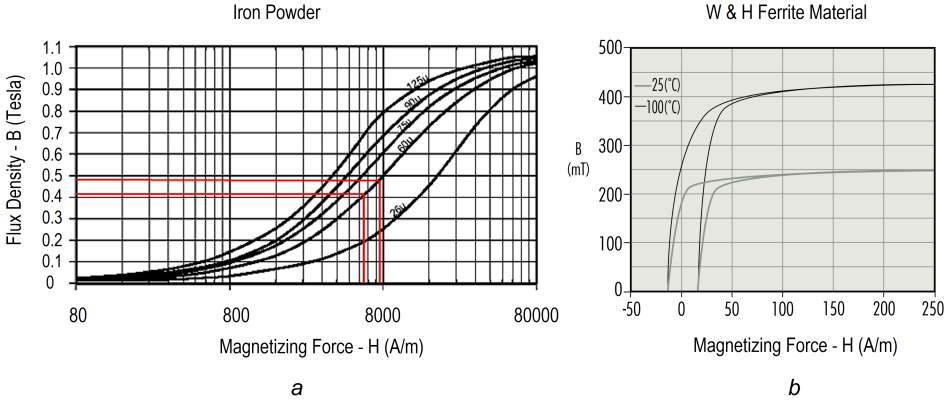

Figure 6. Hysteresis behaviour comparison: (**a**) Hysteresis loop of powdered-iron [21]; and (**b**) Hysteresis loop of W and H ferrites [21].

Moreover, due to the high magnetic reluctance (due to air-gaps inside) of powdered-iron, it has a high remanent flux density that provides a better capacity for flux storage; hence, we argue that the more reluctive powdered-iron shows a stronger magnetic energy storage capability compared to ferrite [24,25]. The coupled-inductor design made using powdered-iron core exhibits unique characteristics during surge propagation by storing surge-related flux that would otherwise be passed directly to the electrical appliance load. However, at the same time, certain drawbacks arise from the coupled-inductor action during transient operation. In the following subsection, we describe how the SCASA performance was lowered due to drawbacks in operation.

3.2. Problems with the Present Design

During the event of an incoming surge, both primary and secondary coils of the coupled-inductor induce opposing voltages to limit surge propagation. According to the design configuration, the secondary induced voltage v_s is always greater than that of the primary v_p. Moreover, both v_s and v_p are generated in the same direction against the incoming transient surge [26].

A clear understanding about the release of these two induced voltages can be obtained by disconnecting the supercapacitor sub-circuit of SCASA main circuit. Accordingly, we observed (Figure 13) that the difference between v_s and v_p ($v_s - v_p$) passes to the load end as a problematic negative voltage peak [26]. Oscilloscope waveforms corresponding to this effect are included under test results (Section 7).

To elevate the performance level, as an alternative, we decided to explore the impact of ferrite cores on the present technique. As discussed in Section 3.1, pure ferrite materials possess a very low energy storage capability; thus, their suitability for surge absorption is limited. Therefore, in order to investigate the use of ferrite cores on SCASA technique, we must first enhance the energy storage capacity of them. Accordingly, the authors decided to incorporate thin air-gaps to the toroidal body of ferrite cores. Apart from achieving similar characteristics to powdered-iron, this new modification of ferrite toroids leads to several positive outcomes by optimizing the overall performance of the SCASA technique. A complete analysis about this advancement is presented in Section 7.

In the next section, we model the equivalent magnetic circuit of an air-gapped toroidal core in order to examine how the relative permeability of an un-gapped core is altered due to an air gap inside. Moreover, we extend our model to show how surge-related magnetic flux can be stored as remanent flux in air-like media.

4. Development of Models for an Air-Gapped Toroid

4.1. Importance of an Air-Gap in Ferrite-Iron

Magnetic permeability is one of the important magnetic characteristics of a material that indicates how easily a material is magnetized [27]. As soft ferrites (W and H ferrites) have high relative permeabilities, they can be magnetized and demagnetized easily, and their flux-based losses are small [28]. However, soft ferrite materials are resistant to sustain magnetism; thus, they have a very low magnetic energy storage capability with a minor remanence [28].

As previously discussed, coupled-inductor coils that include powdered-iron as the core show a greater capability of absorbing surge energy. Therefore, in adapting this new approach of a ferrite core for the coupled-inductor, we must first ensure that it has sufficient energy storage capability. That led us to insert an air-gap to the ferrite core body by cutting it using a diamond coated blade. This modification elevates the magnetic hardness of the soft ferrite material leading to better energy storage.

4.2. Effective Relative Permeability of an Air-Gapped Core

To predict the variations of permeability of a toroidal core in the presence of an inserted air gap (Figure 7), we construct a reluctance-based equivalent magnetic circuit in which the total magnetic flux Φ(t) equally passes through both the core reluctance $\Re_c$ and air-gap reluctance $\Re_g$. As shown in Figure 8, when the flux passes through, magnetic energy is stored in each of these reluctive components. This modification in total reluctance due to the air-gap is essential for our application; the following equations mathematically describe the effects in detail.

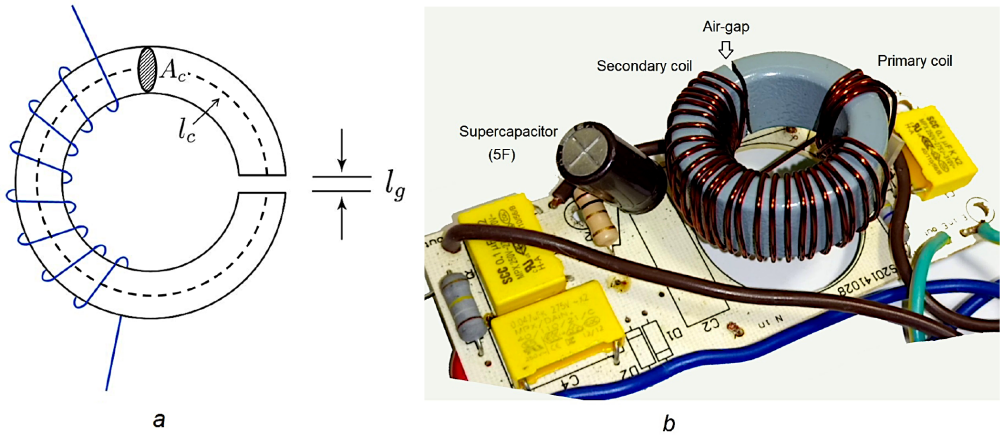

Figure 7. Air-gapped core: geometrical representation vs. physical view: (**a**) Geometrical configurations of a toroidal core with an air-gap [29]; and (**b**) air-gapped ferrite core installed to the SCASA circuit.

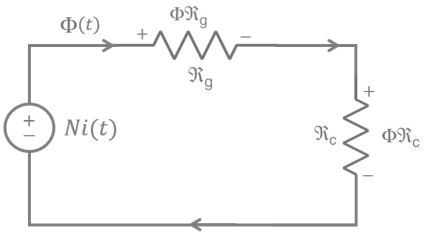

Figure 8. Equivalent magnetic circuit of an air-gapped core.

The total reluctance $\Re_T$ of the core with air-gap is the sum of individual reluctances [30],

$$\Re_T = \Re_c + \Re_g \tag{6}$$

$$\Re_T = \frac{l_c}{\mu_c A_c} + \frac{l_g}{\mu_\circ A_c} \tag{7}$$

where l_c is circular length of core, l_g is the length of the air-gap, A_c is the core cross-sectional area, μ_c is the permeability of the core, and $\mu_\circ$ is the permeability of free space.

As per the definition of relative permeability $\mu_r = \mu_c/\mu_\circ$, we can rearrange (7) as:

$$\Re_T = \frac{1}{\mu_\circ A_c}\left[\frac{l_c}{\mu_r} + l_g\right] \tag{8}$$

By introducing an effective permeability (μ_l) to the core as a whole, the total reluctance can alternatively be written as (9):

$$\Re_T = \frac{l_c + l_g}{\mu_l A_c} \tag{9}$$

From (8) and (9), it is possible to deduce the effective relative permeability ($\mu_l{}'$) of the core in a different manner, and this result shows how the permeability of the air-gapped core varies with the gap length.

$$\mu_l{}' = \frac{\mu_l}{\mu_\circ} = (l_c + l_g)\left[\frac{\mu_r}{\mu_r l_g + l_c}\right] \tag{10}$$

Equation (10) is further simplified by approximating $l_c + l_g \approx l_c$ (since $l_g << l_c$); therefore, (10) reduces into:

$$\mu_l{}' = l_c\left[\frac{\mu_r}{\mu_r l_g + l_c}\right] \tag{11}$$

This result confirms the reduction of permeability in the presence of a reluctive medium such as air [23,31]. When

$$l_g = 0 \rightarrow \mu_l{}' = \mu_r$$

$$l_g > 0 \rightarrow \mu_l{}' < \mu_r$$

Insertion of the air column to the toroid provides a significant reduction in permeability, while enhancing the magnetic energy storage capability [31,32]. As described above, the extra component of reluctance $\Re_g$ added by the air-gap retains more of surge-related flux leading to a better level of surge absorption.

4.3. Reduction of Self-Inductance in the Presence of an Air-Gap

In the previous section, we developed an equation to quantify the drop in magnetic permeability for a core with an air-gap. Here, we extend that analysis to predict the reduction of self-inductance for a coil wound to a similar core. By rearranging (11):

$$\mu_l{}' = \frac{\mu_r}{\left[\mu_r \frac{l_g}{l_c} + 1\right]} \tag{12}$$

A coefficient α can be introduced to the ratio l_g / l_c;

$$\mu_l{}' = \frac{\mu_r}{\left[\mu_r \alpha + 1\right]} \tag{13}$$

By definition [28], self-inductance L_c of a coil wound on an ungapped toroidal core is:

$$L_c = \frac{N^2 \mu_c A_c}{l_g} \tag{14}$$

where $\mu_c = \mu_r \mu_\circ$.

Using (13) and (14), the resulting self-inductance $L_c{}'$ of a coil wound on an air-gapped core can be written as:

$$L_c{}' = \frac{L_c}{\left[\mu_r \alpha + 1\right]} \tag{15}$$

This clearly indicates that $L_c{}'$ always yields a reduced value compared to L_c regardless the value of α. Though a larger α results in significant reduction of $L_c{}'$, we found the optimum energy storage was obtained for α = 0.025 (single-gapped core) and 0.05 (double-gapped core). The theoretical approach used here can be verified with experimental findings taken from SCASA coupled-inductor windings; supporting test results are presented in Section 6.

4.4. Magnetic Energy Stored in an Air-Gap

The main purpose of inserting an air-body into the ferrite core is to enhance its energy storage capacity; as previously mentioned, magnetic energy $E_\circ$ stored in the air-gap helps to reduce surge energy from being transferred to the load side. Using Ampere's law and the flux-based definition of inductance, we derived an expression for $E_\circ$ in [29] as below.

$$E_\circ = \frac{1}{2} \frac{B^2 v_g}{\mu_\circ} \tag{16}$$

where, $v_g = A_c l_g$ is the volume of air-body inside the toroid (Figure 7), and B is the magnetic flux density across the core when a surge current passes through the core windings. Due to leakages and fringing near the air-gap, the surge energy stored is wasted without leading to a release later.

Compared to powdered-iron, which caused a negative surge peak, air-gapped ferrite is advantageous in SCASA design as the lossy effects of surge-flux are dominant. Details about this effect are discussed in Section 7. We now examine the transformer equivalent circuit of SCASA core to establish how various non-ideal parameters vary with the physical modifications made.

5. Equivalent Circuit of SCASA Non-Ideal Transformer and Its Operation

As introduced briefly in Section 3, the transformer core of the SCASA circuit possesses several leakage effects as well as non-infinite magnetizing inductances. Due to these non-ideal characteristics, operation of the circuit deviates from the ideal transformer behaviour. Moreover, reluctance of the core is also dominant due to air-bubbles distributed inside powdered-iron. Similar non-ideal effects are shown by an air-gapped ferrite core, though an ungapped ferrite yields near ideal behaviour. Figure 9 illustrates magnetizing inductances (L_1,L_2) and leakage inductances (l_1,l_2) associated with the primary and secondary coils of the SCASA transformer core.

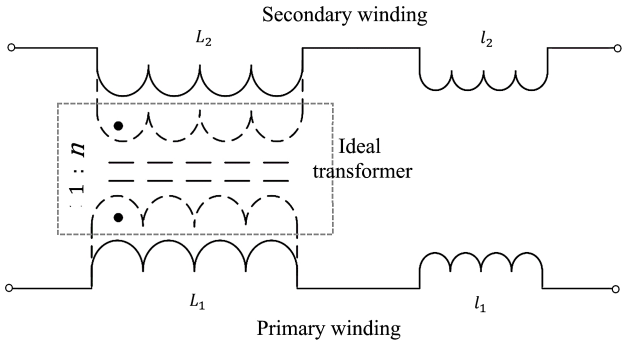

Figure 9. Equivalent circuit of the non-ideal transformer core of SCASA design.

In the transformer circuit shown above, both L_2 and l_2 can be referred to the primary side by dividing them by n^2, where n (N_2/N_1) is the secondary:primary turns ratio. We omitted the winding resistances as their impact on this analysis is negligible. As per the definition of self-inductance [30,33], the total self inductances of primary (L_p) and secondary (L_s) windings are,

$$L_p = L_1 + l_1 \tag{17}$$

$$L_s = L_2 + l_2 \tag{18}$$

By referring all inductive components to the primary, the effective primary referred inductance $L_p{}'$ takes the form:

$$L_p{}' = L_1 + l_1 + L_2/n^2 + l_2/n^2 \tag{19}$$

For the convenience of derivations, we now rearrange our equations using a "permeance"-based approach; permeance is defined as the inductance per unit turn squares ($\Lambda = L/n^2$) [30,34].

If we consider both the magnetizing permeance (Λ_m) and leakage permeance (Λ_σ) separately [30,34], then (17) and (18) can be expressed as:

$$L_p = \Lambda_m {N_1}^2 + \Lambda_\sigma {N_1}^2 \tag{20}$$

$$L_s = \Lambda_m {N_2}^2 + \Lambda_\sigma {N_2}^2 \tag{21}$$

Moreover, magnetic interaction between the two windings depends on the mutual inductance (M) of the core; this can be indicated using Λ_m as per (22).

$$M = \Lambda_m N_1 N_2 \tag{22}$$

In the next section, we investigate how each of these inductive components varies for different toroidal cores: powdered-iron, ferrite-iron, and air-gapped ferrite.

Operational Modes of the Transformer Core

The SCASA equivalent circuit model has two distinct operational modes: a 50 Hz AC steady state, and transient propagation state. As shown in Figure 10, under 230 V AC, neither of the MOVs Var 1 and Var 2 are fired; therefore, both MOVs exhibit open-circuit conditions. Then, if we consider the complete equivalent circuit, the sharing of RMS currents (primary current I_1 and secondary current I_2) depend mainly on the impedance levels. In separate research [35], we determined that nearly 95% of the total RMS current flows through the secondary winding, whereas only 5% passes through the primary winding.

However, circuit operation switches over following the injection of a surge pulse into the power line. In Figure 10, we indicate a surge generation phase using a lightning surge

simulator (LSS-6230). Combinational surge-waveforms (6 kV/3 kA) defined by the IEEE C62.41 standard [36] are injected and superimposed on the AC mains using LSS-6230. Under transient conditions, both MOVs become highly conducting [37]; this state can be indicated by replacing dashed lines (open-circuit stage) with relevant "ON resistances" (R_{ON}) of both varistors.

The most noticeable aspect here is the reversal of current propagation. Contrasting to the 50 Hz RMS conditions, high frequency transients generate greater impedances in transformer windings. Hence, the secondary coil, having more turns, produces a significantly larger impedance than the primary coil. This results in ∼ 60% of i_{surge} passing through the primary and ∼40% through the secondary channel [35].

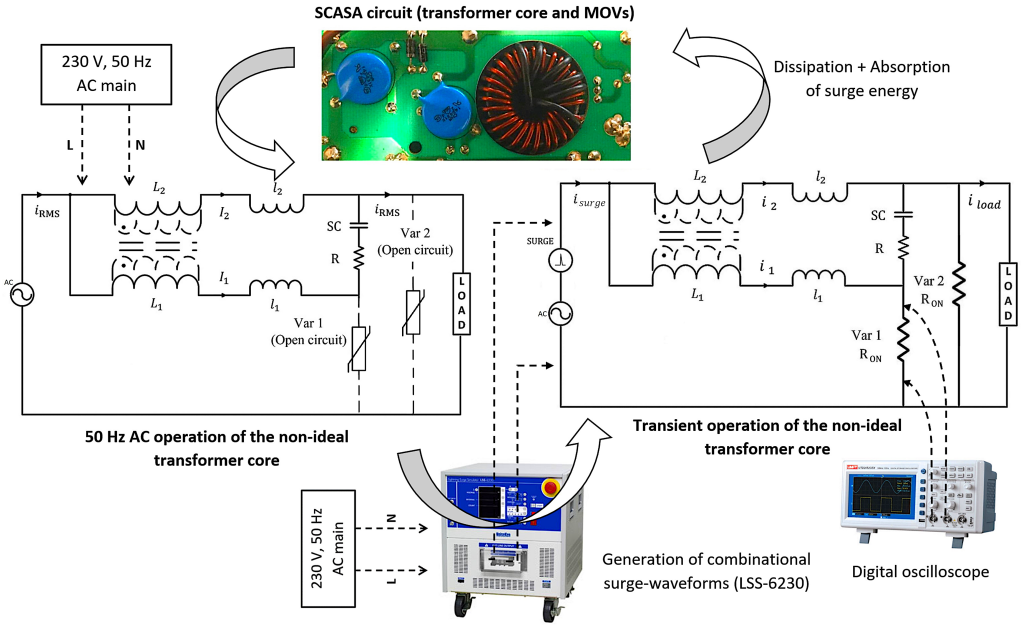

Figure 10. The 50 Hz AC operation and transient-mode operation of SCASA transformer core.

6. Measurements of Non-Ideal Characteristics of SCASA Transformer Core

In Section 5, we discussed details of the equivalent circuit model of magnetic core utilized in SCASA design. As this research aims to optimize the load-side voltage and surge endurance of the present technique, it is important to investigate how circuit parameters change with the selection of core type.

We measured magnetizing and self-inductances along with leakage components of the powdered-iron core. The core of the original SCASA design comprises a powder-iron alloy with two coils (primary and secondary) wound at an unequal number of turns. The primary winding has six turns, whereas the secondary is composed of 28 turns. Inductance measurements of both windings were carried out using a LCR meter (Fluke PM6304) over a range of frequencies from 1 to 15 kHz. Such procedures confirm the accuracy of the test results as frequency components of a 1.2/50 µs surge waveform are significant in the kilohertz range [35,38].

In order to determine leakage inductance of both the primary and secondary, the short-circuit test method was used, whereas the open circuit test procedure was implemented in finding the self-inductances of both windings. By applying series and inverse-series test methods, mutual inductance of the transformer core was obtained [39]. Using the mutual inductance, L_1 and L_2 are easily found (MN_1/N_2 and MN_2/N_1 respectively) [30,39].

Table 1 summarizes the selected measurements taken for the powdered-iron core at 3 kHz; other test results up to 15 kHz are presented in Figure 11. Theoretical predictions in Table 1 were determined as per (20)–(22). According to the manufacturer

(Magnetics Inc.) specifications of the powdered-iron core, $\Lambda_m = 61 \pm 8\%$ nH/turn^2 and $\Lambda_\sigma = 42 \pm 8\%$ nH/turn^2 [40].

Table 1. Magnetizing and leakage inductances of the powdered-iron core (0077071A7).

Inductance	Measurement (μH)	Model Prediction (μH)	Percentage Variation
L_1	2.12	2.2	∼4%
l_1	1.6	1.6	0%
L_2	46.1	47.8	∼4%
l_2	34.6	34.98	∼1%
M	9.88	9.9	∼0.2%

Next, we investigated how SCASA technique performs when the powdered-iron core is replaced with a ferrite core. We selected ZW43615TC, a W-ferrite based toroid that has a similar geometry as the original powdered-iron core with the cross sectional areas and internal diameters of both cores being approximately equal. However, ZW43615TC core possesses an extremely high relative permeability (μ_r = 10,000) [22], far greater than the permeability of 0077071A7 (μ_r = 60). In addition, the pure ferrite inductor has a very large inductance due to its high permeability.

This is a drawback to surge protection since it results in a significant impedance that hinders 50 Hz AC transfer. Another drawback is that ferrite materials have very limited energy storage (Figure 6). By reducing permeability and improving energy storage, we aim to devise a modified ferrite core that has superior characteristics to powered-iron. Hence, as a satisfactory modification, as predicted in Section 4, we decided to incorporate air-gaps into the ferrite core (Figure 7).

Two main approaches were considered here. One was to insert a single air-gap of length l_g (2 mm), and the other was to double the effect by inserting two air-gaps on opposite sides. It was experimentally challenging to cut pure ferrite due to its brittleness; therefore, grinding tools with diamond coated blades were used to insert fine cuts in both cases.

As indicated earlier, different parameters of our circuit model (Figure 9) vary in the presence of different core types. Therefore, to visualize these variations, we plotted self-inductances and leakage inductances of both core windings over a range of frequencies. Figure 11 compares the inductances for the four toroidal cores under test. Measurements from open-circuit tests (self-inductance) are presented in Figure 11a,b; whereas, measurements from short-circuit tests (leakage inductance) are illustrated in Figure 11c,d.

According to Figure 11a, the secondary winding yielded a significantly larger self-inductance when a pure ferrite material (ZW43615TC) was used as the inductor-base; however, the opposite characteristics were observed when wound on the powdered-iron core. This observation remained steady throughout the full frequency range. Consistent with their contrasting permeabilities, ferrite and powder-iron are expected to have a substantial difference in their measured inductance. Moreover, ferrite cores with air-gaps exhibited significant drops in secondary inductance. The double-gapped core showed an inductance reduced to the same level as powdered core, while the single-gapped ferrite core recorded a moderate inductance.

This pattern continued for the primary winding self-inductance (Figure 11b). It is notable that three out of the four main core types (powdered-iron, single-gapped, and double-gapped ferrite) exhibited similar inductance characteristics with a minimum disparity; this phenomenon was observed throughout the frequency range. More importantly, Figure 11b further justified how close the self-inductance was for the doubled-gap core in comparison with powdered-iron core.

$$\text{Leakage percentage} = \frac{\text{Leakage inductance}}{\text{Self inductance}} \times 100\% \tag{23}$$

In the context of leakage inductance analysis, it is hard to identify a clear pattern between primary and secondary windings. Since leakage depends on the core dimensions and availability of air gaps, we see that, as expected, the doubled-gap core displayed elevated leakage inductances in Figure 11d. As per (20) and (21), leakage is a component of self-inductance; hence, the core that yielded the largest secondary self-inductance showed the greatest leakage level (Figure 11c). However, to obtain a better picture of the leakage levels, we extended our study by considering a percentage analysis as given by (23).

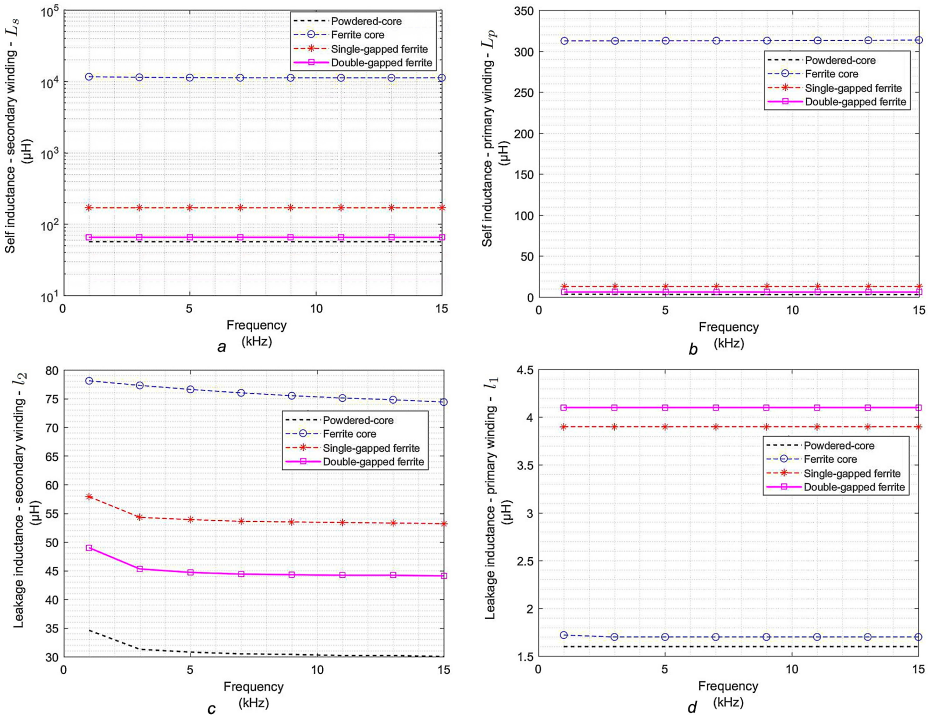

Figure 11. Comparison of the self and leakage inductances of primary and secondary windings for the four core types under test: (**a**) Variation of self-inductance of secondary; (**b**) Variation of self-inductance of primary; (**c**) Variation of leakage-inductance of secondary; (**d**) Variation of leakage-inductance of primary.

Figure 12 reveals consistent leakage percentages for the two windings. In both cases, similarities are seen. According to Figure 12a,b, it is clear that the unmodified ferrite core has almost zero leakage percentage, supporting a strong magnetic coupling between the two coils. Despite that, as pure ferrite cores shows poor energy storage capability, primary and secondary coils fail to capture much of the surge energy passing to the load.

With the insertion of air-gaps, we aimed at increasing leakage levels, and this was validated by the test measurement with both the primary and secondary windings exhibiting significant increments. Accordingly, the double-gapped core was the most dominant with about 65–70% leakage (Figure 12a,b) compared to ∼30% for the single-gapped core. These observations remained steady for the full frequency range considered. The powdered-iron core showed leakage values around 55% and 60% for the primary and secondary, respectively.

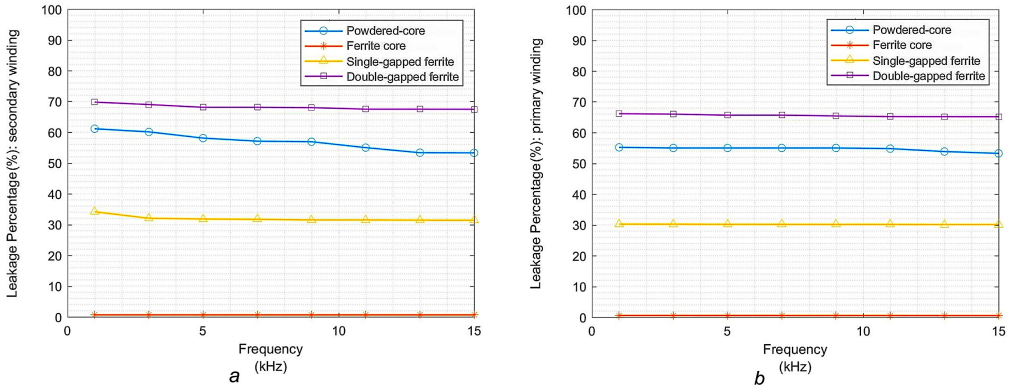

Figure 12. Comparison of the leakage percentages of primary and secondary windings for the four core types under test: (**a**) Leakage percentage analysis of secondary winding; (**b**) Leakage percentage analysis of primary winding.

Increased leakage is a positive aspect in surge protection circuits. The key idea is to store and leak the surge-related magnetic flux during immediate propagation of a transient surge to protect the critical load. Therefore, the measurements in Figure 12 justify our motivation in designing SCASA prototypes using air-gapped ferrite cores. We discuss further the benefits of this design change in the next section.

7. Comparison of Performance: Powdered-Iron Core vs. Air-Gapped Ferrite Cores

This research was carried out to optimize the overall performance of SCASA device. Improving the load-side voltage and advancing its surge endurance capacity were the two main gaols. Here, we explore how each magnetic-core type meets those goals by comparing their performance under transient operation.

7.1. Improvements to the Load Voltage

In Section 3.2, we examined a drawback of the existing SCASA topology: during transient events, a reverse-sided voltage peak (a negative surge) was observed at the load end. This effect is a direct result of the energy stored inside the core being released immediately after the propagation of a surge pulse. Energies stored in primary and secondary windings of SCASA core develop the voltages v_p and v_s, respectively; hence, during the instantaneous release, the voltage difference (v_s–v_p) is what we see as the negative peak at the load.

According to Figures 5 and 10, it can be noted that varistor 2 (Var2) and load share similar patterns for voltage fluctuations; therefore, by capturing the voltage variation across Var2, it is possible to get a picture of this effect. However, due to parasitic inductances and capacitances, load and Var2 do not see identical voltages; more details regarding this implication are discussed at the end of Section 7.2.

As shown in Figure 10, when SCASA is coupled with 230 V AC, and when a surge of 6 kV is injected, both MOVs (Var1 and Var2) provide clamping to protect the load. In order to capture clamped voltages, we used a digital oscilloscope with 100 MHz bandwidth and 1 GS/s sample rate (Tektronix-TPS2014). Figure 13 illustrates several oscilloscope waveforms obtained for different core types tested. According to Figure 13a (captured for powdered-iron), when the surge current (i_{surge}) and surge voltage (V_{surge}) rise, both MOVs enter into clamping phase and exceed their breakdown voltages. However, as powdered-iron retains and releases more surge energy than any other core, a negative surge of significant magnitude (−860 V) is observed in Figure 13a.

Table 2 summarizes essential details corresponding to all waveforms presented in Figure 13. In the case of ferrite core, an approximately 95% reduction was recorded (Figure 13b). However, our measures to reduce the impact of negative peak have to be very selective to avoid limiting the overall energy storage capability of SCASA. Since pure ferrite possesses a poor flux storage, though it showed a reduced peak, we can eliminate

the possibility of using the ZW43615TC un-gapped core for further improvements. More information about its disadvantages is presented in the destructive test summary (Table 3).

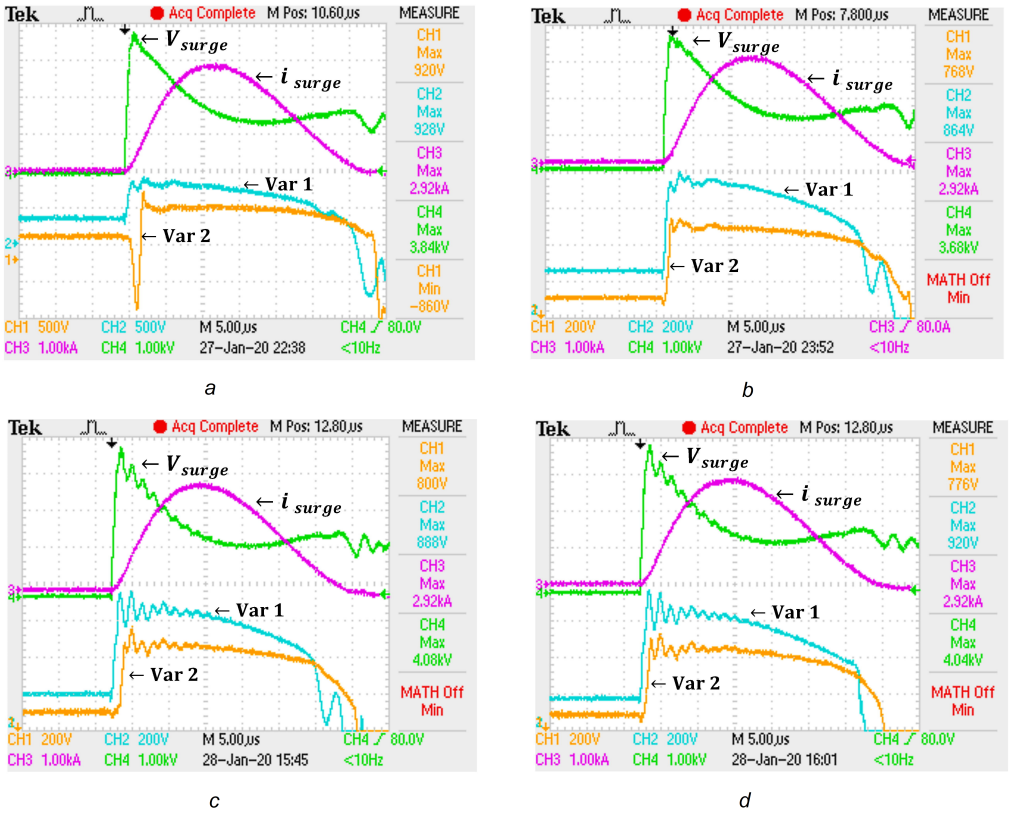

Figure 13. Oscilloscope waveforms for different cores under a transient of 6 kV/3 kA: (**a**) powdered-iron core (0077071A7); (**b**) ferrite-iron core (ZW43615TC); (**c**) single-gapped ferrite core; and (**d**) double-gapped ferrite core.

Table 2. Comparison of negative surge reduction by different core types.

Magnetic Core Type	Magnitude of Negative Surge Passing to the Load (V)	Amount of Negative Surge Reduced (V)	Reduction Percentage
Powdered-iron (0077071A7)	−860	0	0%
Ferrite (ZW43615TC)	−40	820	~95%
Single-gapped Ferrite	−20	840	~98%
Double-gapped Ferrite	−20	840	~98%

Table 3. Destructive testing summary: surge endurance assessment according to the UL-1449 test standards.

Magnetic Core Type	Observations When Subjected to 200 Consecutive Surges	Clamping Voltage after 200 Surges	Impact of Negative Surge (Load-End)
Powdered-iron (0077071A7)	MOVs withstood surge energy (Clamping achieved)	∼950 V	Observed (−900 V)
Ferrite (ZW43615TC)	Failed (Failure of Var1)	Failed	Failed
Single-gapped Ferrite	MOVs survived (Improved clamping)	∼800 V	∼95% reduction (−20 V to −40 V)
Double-gapped Ferrite	MOVs survived (Improved clamping)	∼770 V	∼95% reduction (−20 V to −40 V)

Next, similar oscilloscope waveforms were captured for the air-gapped ferrite cores. As previously discussed, by incorporating air-gaps, we aimed at enhancing the flux absorbing capacity; air-columns potentially store surge-related magnetic flux and, then, release stored energy to the environment without passing to the load-side. Alternatively, the magnetic reluctance of the core-material increases due to air-gaps (Figure 8); hence, the core itself is turning to a lossy medium with greater residual capacity. Figure 13c,d reflects these advancements as the negative surge-peak reduces by approximately 98% in the case of single-gapped and double-gapped ferrite cores (Table 2). This is a substantial reduction of about 820 V as the initial –860 V peak drops to –20 V.

SPDs are primarily characterized by their clamping-voltage level. Lower clamping indicates better surge absorption and, hence, more protection. Therefore, we analysed how the clamping levels varied for the different core types; a comparison is presented in Table 3. Here, voltages across both MOVs of SCASA circuit (Var1 and Var2) were considered (Figure 13). However, Var2 is of greater concern as the load-end is directly connected to it.

In the present SCASA design built using a powdered-iron core, a clamping level of about 920 V was noticed, and, in comparison, all ferrite-based cores yielded much lower clamping voltages. However, as we eliminated the use of un-gapped ferrite toroid (ZW43615TC) in our application, it is important to compare the reduction levels of two air-gapped approaches. The single-gapped core showed an encouraging 120 V reduction in clamping voltage, which is a 13% reduction compared to powdered-iron. Moreover, the double-gapped core recorded a promising drop of 144 V and clamping voltage of around 776 V. This is a significant improvement to the Var2 voltage, and is a 16% reduction (Table 3) from the initial 920 V.

The test results thus far validated our attempts to optimize the overall surge absorption capability of SCASA technique. Substantial improvements in load/Var2 voltage were recorded with the elimination of a negative surge-peak and with a lower level voltage-clamping. Next, we extend our investigation with a destructive testing method.

7.2. Evaluation of Surge Endurance

An essential attribute of any SPD is its durability; depending on the level of endurance a SPD shows under consecutive transient surges, we can assess how resilient it is against surges. Thus, final performance evaluation tests of SCASA were conducted according to the international standards of Underwriters Laboratories (UL-1449 3rd edition) [41]. A simplified version of this procedure is demonstrated in Figure 14.

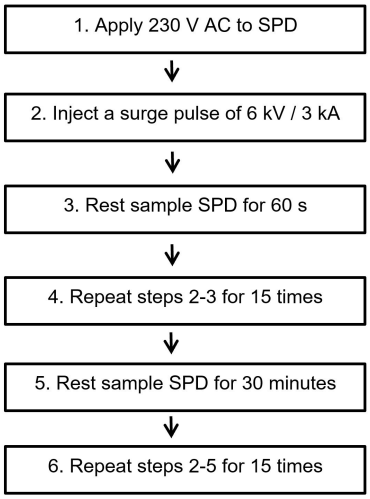

Figure 14. UL-1449 third edition test procedure.

Under this test method, combinational surge-waveforms (6 kV/3 kA) are consecutively injected to the AC mains using a lightning surge simulator; in the meantime, SPD is kept coupled with the AC mains (Figure 10). Sufficient rest periods of 60 s and 30 min were provided throughout the procedure to allow the dissipation of heat. Consecutive surge generation was achieved by means of repeating several steps. The pass criteria for this test is that the sample SPD must still function at the nominal system and that the clamping voltage is still achieved at the end. UL-1449 test method is a form of destructive testing as, at times, protection circuits fail to withstand the continuous application of surges.

According to the summary given in Table 4, we can further verify why un-gapped ferrite toroid is not applicable for SCASA technique. In Section 7.1, we described that, due to the poor energy storage capability of ZW43615TC, its usability in surge protection circuits is highly limited. Hence, during the transient propagation, more surge energy passes to the Var1 via less inductive primary winding. This results in blowing up the Var1 prior to the 200-surge mark; accordingly, we can notice a failure in clamping and a negative surge reduction.

Table 4. Comparison of the clamping level reductions from different core types.

Magnetic Core Type	Clamping Voltage of Var2 (V)	Reduction of Clamping Voltage (V)	Reduction Percentage
Powdered-iron (0077071A7)	920	0	0%
Ferrite (ZW43615TC)	768	152	∼17%
Single-gapped Ferrite	800	120	∼13%
Double-gapped Ferrite	776	144	∼16%

Despite that, other three core types (powdered-iron and two air-gapped cores) indicated success by passing the test criterion of UL-1449. In all three cases, Var1 and Var2 of the SCASA circuit withstood the surge energy without failing prior to the 200-surge mark. However, by comparing the powdered-iron based SCASA prototype with two air-gapped approaches, we can clearly identify two major improvements. Optimized clamping levels were recorded in both single-gapped and double-gapped cores with approximately 800 V and 770 V; whereas, the powdered-iron core still showed a high clamping of 950 V.

All the above clamping voltages were monitored across Var2; however, the load voltage was 50–70 V lower than that in each case due to parasitic inductances/capacitances of the circuit path. We experimentally verified this phenomenon for 6 kV and found it as a useful voltage reduction mainly due to SCASA's 1.2-m long power outlet cable. Overall,

the improved SCASA circuit can prevent sensitive load equipments from being damaged as most household appliances have a surge-immunity level up to 700 V [42].

Another encouraging advancement of the two air-gapped cores was the elimination of the negative surge-peak. Apart from withstanding 200 test surges, both single-gapped and double-gapped toroids revealed a promising ∼95% reduction of the negative-surge effect at load-end. As explained in Section 7.1, by leaking the stored surge-energy instead of passing it to the load side, the ferrite cores with air-gaps yielded better performance than the powdered-iron core.

8. Conclusions

This paper demonstrated improvements to the patented SCASA technique with two significant advances: elimination of the negative surge-peak that passes to the load-end during transient-mode operation, and reduction of the clamping voltage across the sensitive load. As validated by the test results, both improvements were achieved by utilizing air-gapped ferrite cores for the SCASA transformer. Quantitatively, there was a 95% reduction of the negative-surge effect, and a promising 13–16% depletion in the clamping level. Theoretical work based on magnetic permeance provides a useful model for understanding various non-ideal transformer characteristics. All theoretical predictions were found to be within 5% agreement with LCR-meter measurements.

During the final destructive testing conducted according to UL-1449 test-protocols, we observed better surge-endurance levels for the SCASA prototypes that utilized air-gapped cores. Throughout the experimental phase, consecutive surge pulses of combinational waveforms (6 kV/3 kA) were generated using a lightning surge simulator coupled with the AC main.

In future research work, we aim to model the surge-current propagation through SCASA core windings using the Laplace transform method. Furthermore, we are presently working with Magnetics Inc. to test the potential core samples based on new magnetic materials, such as "High Flux, X Flux, Edge and Kool Mμ HF", with the expectation of selecting an optimum core material and shape for the SCASA transformer.

Author Contributions: Conceptualization, S.U.S.T.; methodology, S.U.S.T.; software, S.U.S.T.; validation, S.U.S.T.; formal analysis, S.U.S.T.; investigation, S.U.S.T.; resources, S.U.S.T.; data curation, S.U.S.T.; writing—original draft preparation, S.U.S.T.; writing—review and editing, N.K.; supervision, N.K.; writing—review and editing, D.A.S.-R.; supervision, D.A.S.-R. All authors have read and agreed to the published version of the manuscript.

Funding: This research received no external funding.

Institutional Review Board Statement: Not applicable.

Informed Consent Statement: Not applicable.

Data Availability Statement: The data presented in this study are available on request from the author panel. The data are not publicly available due to the commercialization of SCASA technique.

Acknowledgments: The authors would like to thank Bradley M. Yourish, senior vice president of sales and marketing, Magnetics Inc. for providing the magnetic core samples required for SCASA circuit prototypes. We truly appreciate his co-operation in this regard.

Conflicts of Interest: The authors declare no conflict of interest.

Abbreviations

The following abbreviations are used in this manuscript:

AC	Alternating Current
RMS	Root Mean Square
SC	Supercapacitor

SCASA	Supercapacitor assisted Surge Absorber
SPD	Surge Protector Device
SMART TViQ	Commercial Implementation of SCASA Technique
NLD	Non Linear Device
BBD	Bidirectional Break-over Diode
MOV	Metal Oxide Varistor
EC	Electrolytic Capacitor
EDLC	Electric Double Layer Capacitor
Var1 and Var2	Varistor 1 and Varistor 2
ITRS	International Technology Roadmap for Semiconductors

References

1. IRDS. *The International Roadmap for Devices and Systems (IRDS): Beyond CMOS*; Technical Report; European Semiconductor Industry Association, Institute of Electrical and Electronics Engineers: Piscataway Township, NJ, USA, 2020.
2. Batarseh, I.; Harb, A. *Power Electronics: Circuit Analysis and Design*; Springer International Publishing: Cham, Switzerland, 2017.
3. IEC 60038:2009. *IEC Standard Voltages*; International Electrotechnical Commission: Geneva, Switzerland, 2009.
4. Laughton, M.A.; Warne, D.F. *Electrical Engineer's Reference Book*; Elsevier Science: Burlington, MA, USA, 2003.
5. Mullin, R.C.; Simmons, P. *Electrical Wiring Residential*, 20th ed.; Cengage Learning: Boston, MA, USA, 2021.
6. Dranetz, T. *The Dranetz Field Handbook for Power Quality Analysis*; Dranetz Technologies Incorporated: Brockton, MA, USA, 2020.
7. Barnes, J.R. (Ed.) Transient Suppressors and Surge Suppressors. In *Robust Electronic Design Reference Book*; Springer: Berlin/Heidelberg, Germany, 2019.
8. Lee, B. Surge Protection Device. US Patent 4,901,183. Available online: https://www.google.com/patents/US4901183 (accessed on 20 October 2019).
9. 'IEEE Guide for the Application of Surge-Protective Components in Surge-Protective Devices and Equipment Ports–Overview', IEEE Standard C62.42.0-2016 (Revision of IEEE C62.42-2005). 2017. Available online: https://ieeexplore.ieee.org/document/8016718 (accessed on 20 October 2018).
10. Littlefuse Varistors—Basic Properties, Terminology and Theory. Application Note, July 1999, AN9767.1. Available online: https://www.littelfuse.com/~/media/electronics_technical/application_notes/varistors/littelfuse_varistors_basic_properties_terminology_and_theory_application_note.pdf (accessed on 14 November 2018).
11. Kularatna, N. *Power Electronics Design Handbook*; Elsevier-Newnes: Burlington, MA, USA, 2006.
12. Kularatna, N.; Ross, A.S.; Fernando, J.; James, S. *Design of Transient Protection Systems* Elsevier: Amsterdam, The Netherlands, 2019; pp. 1–16.
13. Kularatna, N.; Fernando, J.; Pandey, A.; James, S. Surge capability testing of supercapacitor families using a lightning surge simulator. *IEEE Trans. Ind. Electron.* **2011**, *58*, 4942–4949. [CrossRef]
14. Fernando, J.; Kularatna, N. A Supercapacitor Based Enhancement Technique for Stand-Alone Surge Protection Circuits. In Proceedings of the 2013 IEEE International Symposium on Industrial Electronics, Taipei, Taiwan, 28–31 May 2013.
15. Fern, O.J.; Kularatna, N.; Round, H.; Tálele, S. Implementation of the Supercapacitor-Assisted Surge Absorber (SCASA) Technique in a Practical Surge Protector. In Proceedings of the IECON 2014—40th Annual Conference of the IEEE Industrial Electronics Society, Dallas, TX, USA, 29 October–1 November 2014.
16. Kularatna, N. Supercapacitors Improve the Performance of Linear Power-Management Circuits: Unique New Design Options When Capacitance Jump from Micro-Farads to Farads with a Low Equivalent Series Resistance. *IEEE Power Electron. Mag.* **2016**, *3*, 45–59. [CrossRef]
17. Thor Technologies—STViQ/3 SMART TViQ. 2018. Available online: https://www.thortechnologies.com.au/product/stviq3/ (accessed on 22 November 2019).
18. Jayalakshmi, M.; Balasubramanian, K. Simple Capacitors to Supercapacitors—An Overview. *Int. J. Electrochem. Sci.* **2008**, *3*, 1196–1216.
19. Fernando, J. Supercapacitor-Assisted Surge Absorber (SCASA) and Supercapacitor Surge Modelling. Ph.D. Thesis, The University of Waikato, Hamilton, New Zealand, 2016.
20. Magnetics—Powder Core Documents, Mag-inc.com. Available online: https://www.mag-inc.com/Design/Technical-Documents/Powder-Core-Documents (accessed on 18 November 2020).
21. Magnetics—Ferrite Core Documents, Mag-inc.com. Available online: https://www.mag-inc.com/Design/Technical-Documents/Ferrite-Core-Documents (accessed on 6 July 2021).
22. Magnetics—W Material, Mag-inc.com. 2020. Available online: https://www.mag-inc.com/Products/Ferrite-Cores/W-Material (accessed on 26 January 2020).
23. McLyman, C.W.T. *Transformer and Inductor Design Handbook*, 4th ed.; Taylor & Francis: Boca Raton, FL, USA, 2017.
24. Weik, M.H. Magnetic Reluctance. In *Computer Science and Communications Dictionary*; Springer: Berlin/Heidelberg, Germany, 2001.
25. Magnetic Circuit, En.wikipedia.org. 2020. Available online: https://en.wikipedia.org/wiki/Magnetic_circuit (accessed on 24 January 2020).

26. Fernando, J.; Kularatna, N. Supercapacitor Assisted Surge Absorber (SCASA) Technique: Selection of Supercapacitor and Magnetic Components. In Proceedings of the 2014 IEEE Energy Conversion Congress and Exposition (ECCE), Pittsburgh, PA, USA, 14–18 September 2014.
27. Heck, C. (Ed.) 3-Magnetic Parameters of Materials. In *Magnetic Materials and Their Applications*; Elsevier: Amsterdam, The Netherlands, 2014.
28. Snelling, E.C. *Soft Ferrites: Properties and Applications*; Butterworth-Heinemann: Oxford, UK, 2005.
29. Udayanga, S.T.S.; Kularatna, N.; Steyn-Ross, D.A. Investigating the Impact of Ferrite Magnetic Cores on the Performance of Supercapacitor Assisted Surge Absorber (SCASA) Technique. In Proceedings of the 2019 IEEE 28th International Symposium on Industrial Electronics (ISIE), Vancouver, BC, Canada, 12–14 June 2019; pp. 130–135
30. Valchev, V.C.; Van den Bossche, A. *Inductors and Transformers for Power Electronics*; CRC Press: Boca Raton, FL, USA, 2018.
31. Air Gapped Magnetic Cores, Surrey.ac.uk. 2011. Available online: http://info.ee.surrey.ac.uk/Workshop/advice/coils/gap/index.html (accessed on 20 January 2020).
32. Hurley, W.G.; Wölfle, W.H. *Transformers and Inductors for Power Electronics: Theory, Design and Applications*; Wiley: Hoboken, NJ, USA, 2013.
33. Whitaker, J.C. *The Electronics Handbook*; CRC Press: Boca Raton, FL, USA, 2018.
34. Karapetoff, V. *The Magnetic Circuit—Electromagnetic Engineering*; Creative Media Partners, LLC: Sacramento, CA, USA, 2018.
35. Udayanga, S.T.S.; Kularatna, N.; Steyn-Ross, D.A. Permeance based model for the coupled-inductor utilized in the supercapacitor assisted surge absorber (SCASA) and its experimental validation. In Proceedings of the 2020 IEEE 2nd International Conference on Industrial Electronics for Sustainable Energy Systems (IESES), Cagliari, Italy, 1–3 September 2020.
36. 'IEEE Recommended Practice on Characterization of Surges in Low-Voltage (1000 V and Less) AC Power Circuits', IEEE Standard C62.41.2-2002. 2003. Available online: https://ieeexplore.ieee.org/document/1196924 (accessed on 26 January 2019).
37. James, S. Investigation of Surge Propagation in Transient Voltage Surge Suppressors and Experimental Verification. Ph.D. Thesis, The University of Waikato, Hamilton, New Zealand, 2014.
38. Martinez-Velasco, J.A. *Transient Analysis of Power Systems: A Practical Approach*; Wiley: Hoboken, NJ, USA, 2020.
39. Kazimierczuk, M.K. *High-Frequency Magnetic Components*; Wiley: Hoboken, NJ, USA, 2011.
40. Magnetics—Kool Mu Powder Cores, Mag-inc.com. 2018. Available online: https://www.mag-inc.com/products/powder-cores/kool-mu-cores (accessed on 26 January 2020).
41. UL 1449. *UL Standard for Surge Protective Devices*, 3rd ed.; Underwriters Laboratories Inc.: Brooklyn, IL, USA, 2006.
42. *BEAMA Guide to Surge Protection Devices (SPDs)—Selection, Application and Theory*; Industry Report; British Electrotechnical and Allied Manufacturers Association: London, UK, 2018.